mater.scichina.com link.springer.com

Published online 25 November 2021 | https://doi.org/10.1007/s40843-021-1821-4
Sci China Mater 2022, 65(3): 675–682

High-performance proton-conducting solid oxide fuel cells using the first-generation Sr-doped $LaMnO_3$ cathode tailored with Zn ions

Shuai Wu[1,3†], Xi Xu[2†], Xiaomei Li[1,3] and Lei Bi[1*]

ABSTRACT **Sr-doped $LaMnO_3$ (LSM) which is the first-generation cathode for solid oxide fuel cells (SOFCs) has been tailored with Zn ions, aiming to achieve improved protonation ability for proton-conducting SOFCs (H-SOFCs). The new Sr and Zn co-doped $LaMnO_3$ (LSMZ) can be successfully synthesized. The first-principle studies indicate that the LSMZ improves the protonation of LSM and decreases the barriers for oxygen vacancy formation, leading to high performance of the LSMZ cathode-based cells. The proposed LSMZ cell shows the highest fuel cell performance among ever reported LSM-based H-SOFCs. In addition, the superior fuel cell performance does not impair its stability. LSMZ is stable against CO_2, as demonstrated by both *in-situ* CO_2 corrosion tests and the first-principles calculations, leading to good long-term stability of the cell. The Zn-doping strategy for the traditional LSM cathode with high performance and good stability brings back the LSM cathode to intermediate temperatures and paves a new way for the research on the LSM-based materials as cathodes for SOFCs.**

Keywords: $LaMnO_3$, proton-conducting oxides, solid oxide fuel cell

INTRODUCTION

The current mission of reducing CO_2 production requires new technologies to generate electricity with high efficiency and low impact to the environment. Solid oxide fuel cells (SOFCs) that can directly convert chemical energies into electricity answer this call [1]. Recently, proton-conducting SOFCs (H-SOFCs), which use proton-conducting oxides as the electrolyte, become an important research direction in the fuel cell community as they inherit the advantages of traditional SOFCs (such as the all-solid-state structure), while avoiding the high operating temperatures and the dilution of fuels for traditional SOFCs [2]. The research on H-SOFCs has been flourishing in the past few years as they show tremendous potential in intermediate-temperature operations [3]. The performance of H-SOFCs has increased from tens of mW cm^{-2} up to 1 W cm^{-2} in the past decade, nearly catching up with the performance of oxygen-ion conducting SOFCs (O-SOFCs) [4,5]. Generally, there are two strategies for enhancing the performance of H-SOFCs. One is optimizing the microstructure, including the use of thin-layer electrolytes to reduce the ohmic resistance of the cell or/and the utilization of the nanometric electrode for extending the active reaction area [6,7]. The other is the development of new electrolytes with high ionic conductivity at intermediate temperatures [8] and electrode materials with good catalytic activities [9,10], meeting the demand of intermediate-temperature operations. Compared with the anode material, which normally consists of Ni-based cermet [11], the development of cathode materials is a hot topic in the H-SOFC field [12]. It has been found that the cathode influences the overall fuel cell performance more than the anode, and the recently reported high-performance H-SOFCs are usually associated with the design of new cathode materials [13].

Although different cathode materials have been proposed for SOFCs, Sr-doped $LaMnO_3$ (LSM), which is the first-generation cathode material, has been intensively studied, and now it has been used for commercial purposes due to its good stability [14,15]. However, the pure electron-conducting nature of LSM makes it difficult for intermediate-temperature operations [16]. Lots of attempts have been made to utilize LSM-based materials at intermediate temperatures and some achievements have been reported for O-SOFCs [17,18]. However, the use of LSM for H-SOFCs is still challenging. Previous reports indicate the performance of H-SOFCs using LSM cathode is low due to the very low ionic conductivity of LSM at intermediate temperatures [19]. In this case, the triple-phase boundary (TPB) is restricted at the LSM and electrolyte interface, limiting the cathode reaction. The performance of the H-SOFC using LSM cathode can be improved by the impregnation method to form LSM nanoparticles that could extend TPBs and thus enhance the cell performance. However, the fuel cell performance is still moderate, reaching 200 mW cm^{-2} [20], implying further strategies are desired.

Proton migration is involved in the cathode reaction for H-SOFCs, and it is recognized that the promotion of the protonation in the cathode could improve the cathode performance [21]. Incorporating elements with high basicity can improve the protonation of the material [22] but lead to a decrease in chemical stability [23]. Zohourian *et al.* [24] found that the incorporation of Zn at the Fe site of the $BaFeO_3$-based perovskite could enhance the hydration ability of the sample, benefiting the application in H-SOFCs. Although the above study focuses on the $BaFeO_3$-based perovskite, the indication of hydration

[1] School of Resource Environment and Safety Engineering, University of South China, Hengyang 421001, China
[2] Department of Materials, Imperial College London, Prince Consort Road, London SW7 2BP, UK
[3] Institute of Materials for Energy and Environment, College of Materials Science and Engineering, Qingdao University, Qingdao 266071, China
† These authors contributed equally to this work.
* Corresponding author (emails: lei.bi@usc.edu.cn or bilei81@gmail.com)

enhancement by Zn-doping is evident, implying this strategy might also be useful for other ABO_3 perovskite oxides, despite the fact that no such attempt has been made to LSM so far. In addition, the doping of a foreign element into LSM may also influence the electronic structure of the material [25], thus having an evident impact on the catalytic activity of the material and influencing the fuel cell performance. Therefore, this study explores the influence of Zn-doping on the performance of LSM for H-SOFCs by both experimental studies and first-principle calculations, aiming to provide a new LSM-based material for H-SOFCs with high performance and reveal the mechanism for the improved performance.

EXPERIMENTAL SECTION

$La_{0.5}Sr_{0.5}Mn_{0.875}Zn_{0.125}O_{3-\delta}$ (LSMZ) and $La_{0.5}Sr_{0.5}MnO_{3-\delta}$ (LSM) powders were prepared by a conventional wet chemical route with citric acid as the complexing agent, and the preparation details can be found elsewhere [26,27]. Both powders were annealed at 1150°C for 3 h, and the phase purity of the powders was examined by X-ray diffraction (XRD). High-resolution transmission electron microscopy (HR-TEM, JEM-2100F) coupled with the energy-dispersive X-ray spectroscopy (EDS) was used to observe morphologies of the samples as well as the elemental distributions. X-ray photoelectron spectroscopy (XPS) analysis was performed by a Thermo Fisher ESCALAB 250Xi spectrometer using an Al Kα (1486.6 eV) radiation source. The chemical stability tests for LSMZ were carried out with the *in-situ* XRD. Flowing 10% CO_2 was fed into the chamber where the LSMZ was located, and XRD measurements were carried out at the testing temperature to study the stability of the LSMZ. In addition, the tests were held at 600°C for 12 h and continuous XRD measurements were taken during this period to detect the phase of the LSMZ as a function of time at 600°C in CO_2.

To evaluate the performance of LSMZ cathode for H-SOFCs, half-cells using $BaCe_{0.7}Zr_{0.1}Y_{0.2}O_{3-\delta}$ (BCZY) electrolyte and NiO-BCZY anode were prepared by the co-pressing and co-sintering method [28], followed by the deposition of LSMZ-$BaZr_{0.8}Y_{0.2}O_{3-\delta}$ (BZY) composite cathode and co-annealing at 900°C in a microwave furnace. For comparison, LSM cathode without Zn-doping was also deposited on the same half-cell and treated in the same way. The cells were tested with H_2 as the fuel using an electrochemical workstation (Squidstat Plus, Admiral Instrument) with the four-wire method, and the RelaxIS software was used to fit the impedance plot of the cell.

Theoretical calculations were carried out using the density functional theory (DFT) method with the VASP (Vienna *ab initio* simulation package) software [29,30]. All calculations were performed with a cutoff energy for the valence electrons of 500 eV, in a (4 × 4 × 4) gamma centered K-point mesh. The energy and force were converged within 10^{-5} eV and 0.02 eV $Å^{-1}$, respectively. O_2 and CO_2 adsorption energies were calculated by simulating the O_2 or CO_2 adsorption on the LSM and LSMZ surface at the atomic level. A vacuum layer with a thickness of 15 Å was constructed for the surface calculations. The calculation details can be found in our previous studies [31–33].

RESULTS AND DISCUSSION

A wet chemical route was carried out to dope Zn into the LSM lattice, obtaining LSMZ. LSM powders without Zn-doping was prepared in the same way. Fig. 1a shows the XRD patterns of the synthesized LSM and LSMZ. Both samples exhibit a pure perovskite structure without detectable impurities. In addition, the peaks of the LSMZ shift to low angles (Fig. 1b), suggesting the expansion of the lattice which is probably due to the larger ionic radius of Zn^{2+} (74 pm) than that of Mn ion (64.5 pm for Mn^{3+}). The HR-TEM images (Fig. 1c, d) show the *d*-spacing value corresponding to the (002) plane increases from 0.270 nm for LSM to 0.273 nm for LSMZ, indicating an expansion of the lattice, consistent with the result observed from XRD. Further analysis of the LSMZ with scanning TEM (STEM)-mapping as shown in Fig. 1e indicates a homogenous distribution of the elements in the LSMZ powders without obvious element segregations. All the evidence suggests that the Zn ions have been incorporated into the LSM lattice and the LSMZ powders are successfully prepared.

The above study indicates that Zn can incorporate into LSM, forming LSMZ. Therefore, we first evaluate the properties of the material from the atomic point of view. The first-principle calculations have been widely used to investigate and predict the properties of materials, revealing the properties of a specific material at the atomic level and reaching great successes in the past decades. We first compared the properties of the LSM material with and without Zn-doping with the first principle calculations. It is known that the formation of oxygen vacancy (Vo) is critical for both oxygen-ion conduction and proton conduction. The calculation of the Vo formation energy (E_{Vo}) was carried out for both LSM and LSMZ. The E_{Vo} was calculated with the following equation:

$$E_{Vo} = E_{defect} + \frac{1}{2}E_{O_2} - E_{perfect}, \quad (1)$$

where E_{defect} is the total energy of a defective bulk and $E_{perfect}$ is the total energy of the stoichiometric bulk without defects [34]. The E_{Vo} for LSM and LSMZ is 2.14 and 1.01 eV, respectively. The result indicates that the doping of Zn in LSM could significantly lower the E_{Vo}, which benefits the formation of oxygen vacancy. The lower E_{Vo} for LSMZ compared with LSM is expected as the partial replacement of Zn^{2+} for $Mn^{3+/4+}$ could generate extra oxygen vacancies according to the following equations:

$$2ZnO \rightarrow 2Zn'_{Mn} + 2V_O^{\cdot\cdot} + 2O_O^{\times} \text{ (for } Mn^{3+})$$

and

$$ZnO \rightarrow Zn''_{Mn} + V_O^{\cdot\cdot} + O_O^{\times} \text{ (for } Mn^{4+}).$$

The XPS analysis for LSM and LSMZ indicates the increased Vo content by Zn-doping. Fig. S1 (in the Supplementary information) shows the O 1s XPS peaks for LSM and LSMZ, and different oxygen groups can be identified. The ratio of the adsorbed O and lattice O reflects the content of the Vo and the larger ratio means the larger Vo content [35]. The ratio is 1.56 and 1.2 for LSMZ and LSM, as shown in Table S1, suggesting the increase of Vo for LSM with Zn-doping that agrees with the DFT calculations. The iodometric titration method was further employed to measure the oxygen vacancy concentration in LSM and LSMZ. The measured oxygen vacancy concentration in LSM is 0.01 and the value for LSMZ is 0.03, suggesting an increase in oxygen vacancy concentration for LSM by Zn-doping. The improved Vo could promote oxygen diffusion and also facilitate the formation of proton defects.

Protons can incorporate into the oxide lattice when oxygen vacancies are present, according to the reaction:

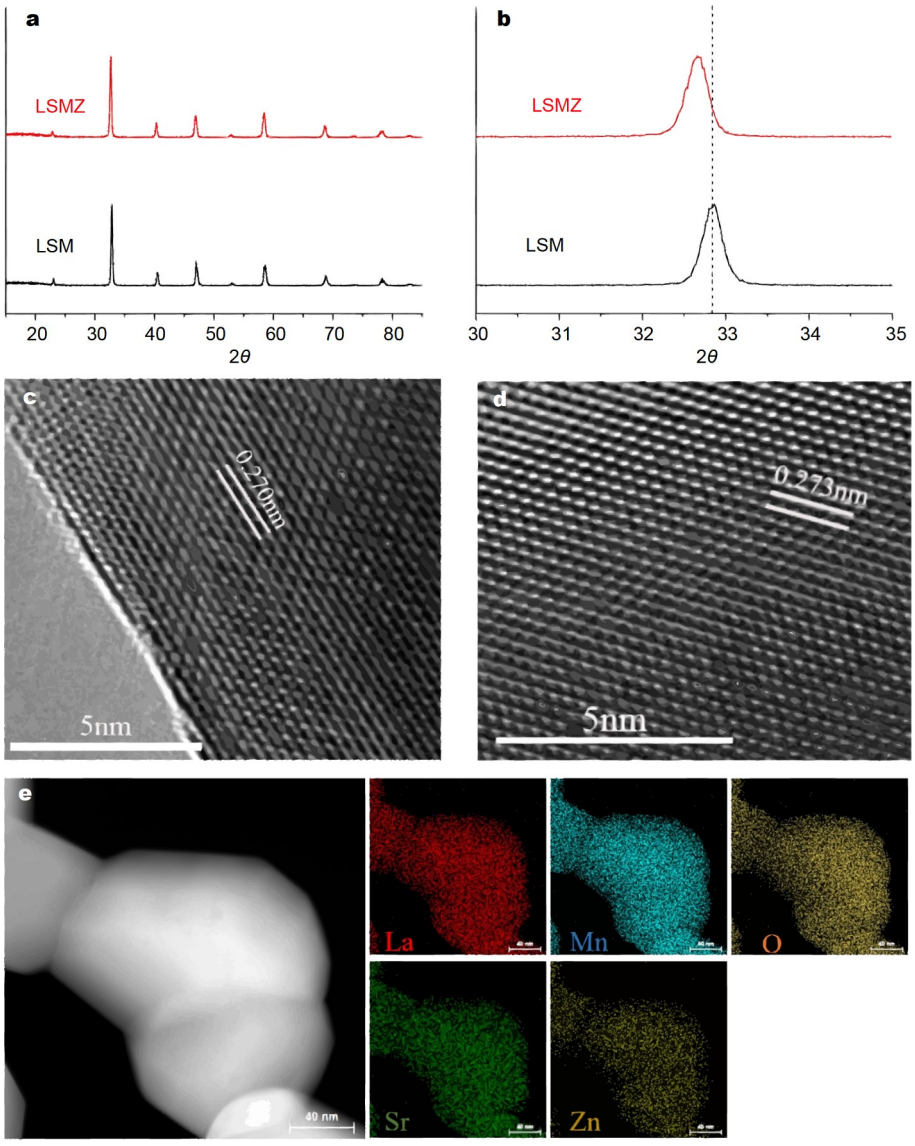

Figure 1 (a) XRD patterns of the synthesized LSM and LSMZ; (b) enlarged view of the XRD patterns; the HRTEM image of (c) LSM and (d) LSMZ; (e) STEM mapping of the LSMZ powders.

$H_2O + V_{\ddot{O}} + O_O^{\times} \Leftrightarrow 2OH^{\bullet}$. Therefore, the hydration energy ($E_{hydration}$) can be calculated with the equation: $E_{hydration} = E_{2OH} - E_{defect} - E_{H_2O}$, in which E_{2OH} is the energy for the hydrated bulk, E_{defect} is the energy for the bulk with one defective oxygen, and E_{H_2O} is the energy for H_2O. The $E_{hydration}$ for LSM and LSMZ is 0.19 and −0.095 eV, respectively. The hydration energy for LSM is above zero, which means the reaction is thermodynamically unfavorable. In contrast, the $E_{hydration}$ is a negative value when ZnO is doped into the LSM lattice, indicating the hydration reaction becomes thermodynamically favorable for LSMZ and the doping of ZnO improves the hydration ability of LSM, which is critical for its application for H-SOFCs. Fig. 2a shows the difference in charge density between LSM and LSMZ. One can see that an apparent charge accumulation for the oxygen atoms close to the Zn ion, suggesting the doping of Zn changes the electronic structure of the material and thus influences the electron density of the neighboring oxygen atoms. The accumulation of charges at the atoms close to the Zn ion suggests a more negative charge for these oxygen atoms, which are more active and tend to incorporate better with protons than the sample without Zn-modification. The electronic change could be the reason for the decreased E_{Vo} and $E_{hydration}$ of the Zn-modified sample. The improvement in hydration ability for LSMZ compared with LSM is also demonstrated by the experimental study. Fig. 2b shows the weight change of LSM and LSMZ between the dry and wet air conditions, indicating the hydration ability of the sample. The hydration ability of the LSM and LSMZ materials was determined by cooling the materials in dry and wet atmospheres and measuring the weight difference in these two atmospheres [36]. As shown in Fig. 2b, LSMZ has a higher hydration ability than that of LSM from 500 to 700°C, consistent with the results from the first-principle calculations. Both the DFT simulation and experimental studies confirm that the doping of Zn into LSM can obviously improve the hydration ability of the sample,

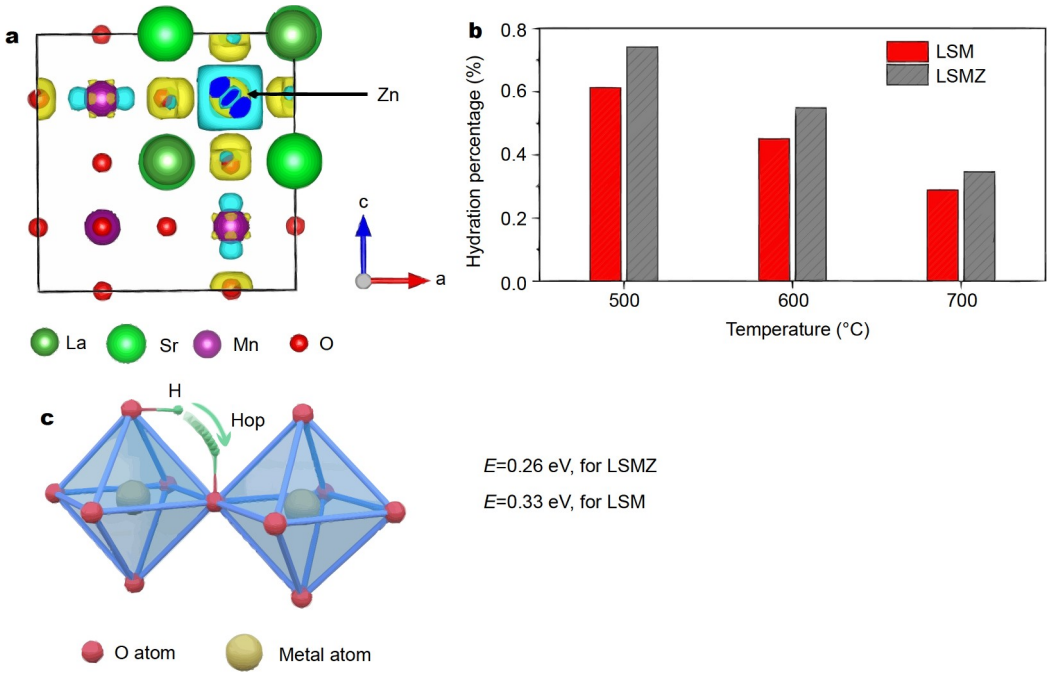

Figure 2 (a) Difference in charge density of LSM after Zn-doping. Blue bubbles mean charge depletion and yellow bubbles mean charge accumulation; (b) the comparison of hydration ability for LSM and LSMZ at different temperatures; (c) scheme for the proton hopping procedure and the calculated proton hopping energy in LSM and LSMZ.

benefiting the protonation of the cathode material and thus could enhance the cathode performance.

The first principle calculations were also performed to predict the proton migration within the oxide. It has been recognized that the proton has to jump from one oxygen atom to the neighboring oxygen atom and the jumping step is usually the rate-limiting step [37]. The jumping energy of protons for LSM and LSMZ is 0.33 and 0.26 eV, as shown in Fig. 2c, indicating the barrier for the proton migration is lowered with Zn-doping and the extra oxygen vacancy in LSMZ does not trap but helps the migration of protons. Therefore, the Zn-doping strategy improves both the oxygen vacancy formation ability and the hydration (protonation) ability of LSM as well as the proton migration ability, making LSMZ a promising cathode for H-SOFCs.

LSMZ was evaluated as a cathode for H-SOFCs, in comparison with traditional LSM cathode. Fig. 3a shows the current-voltage (*I-V*) and power density curves for the H-SOFC based on LSMZ cathode. The peak power density (PPD) of the LSMZ cell is 416, 756, and 1012 mW cm^{-2} at 600, 650, and 700°C, respectively. The PPD values are significantly higher than those of the LSM cell (298, 483, and 622 mW cm^{-2}) tested at the same temperatures (Fig. S2). The composite cathodes were used in this study by coupling the LSMZ/LSM material with BZY in a weight ratio of 7 to 3. LSMZ shows good chemical compatibility with BZY, as no new phase can be detected for the LSMZ-BZY composite powder after annealing at the cathode fabrication temperature (900°C) (Fig. S3). To the best of our knowledge, the current LSMZ cell shows the largest fuel cell performance ever reported for H-SOFCs using LSM-based cathode [19,20,38,39]. Even compared with the advanced microstructure-optimized LSM cathode, the current cell shows much better performance, as indicated in Table 1. One can find that the reports on the use of LSM for H-SOFCs are few due to the instinctive electron-conducting nature of LSM and the low fuel cell performance. Microstructure optimization is currently the only way to improve performance, which heavily relies on the nanostructure of the material at low temperatures, leading to the potential coarsening problem for the cathode particles during the operation and thus to the degradation of the cell performance [17]. The technical difficulties make the direct use of LSM-based material for H-SOFC with high performance necessary and challenging. However, the encouraging performance of the LSMZ cell tackles this problem. The cell performance is even higher than or comparable to some of the recently reported high-performance H-SOFCs based on novel cathodes [5,36,40–47]. The result indicates that the Zn-doping strategy effectively brings LSM back to the intermediate-temperature range with high performance, although LSM is the first-generation cathode that has been regarded only to perform well at high temperatures (above 800°C). In addition, the LSMZ cathode was directly used in this study without the cathode/electrolyte interlayer optimization that can greatly enhance the performance of H-SOFCs [48] and might be used in the future for further enhancing the cell performance. Fig. 3b shows the morphology of the LSMZ cell after testing. The LSMZ cathode is porous, and it adheres well with the BCZY electrolyte without obvious delamination even after testing. The LSM cell (Fig. S4) shows a similar morphology compared with the LSMZ cell. In addition, both cells use identical NiO-BCZY/BCZY half-cells. Therefore, the major contribution for the difference in fuel cell performance is from the cathode material rather than from the cathode morphology or the cell structure. The comparison of electrochemical impedance spectroscopy (EIS) between the LSM and the LSMZ cells is shown in Fig. 3c. One can see that both cells have a similar ohmic resistance (R_{ohmic}) which is about 0.18 Ω cm^2 at 700°C (Fig. 3d). In contrast, the polarization resistance (R_p) of the two cells shows a big difference. The R_p for the LSM cell is

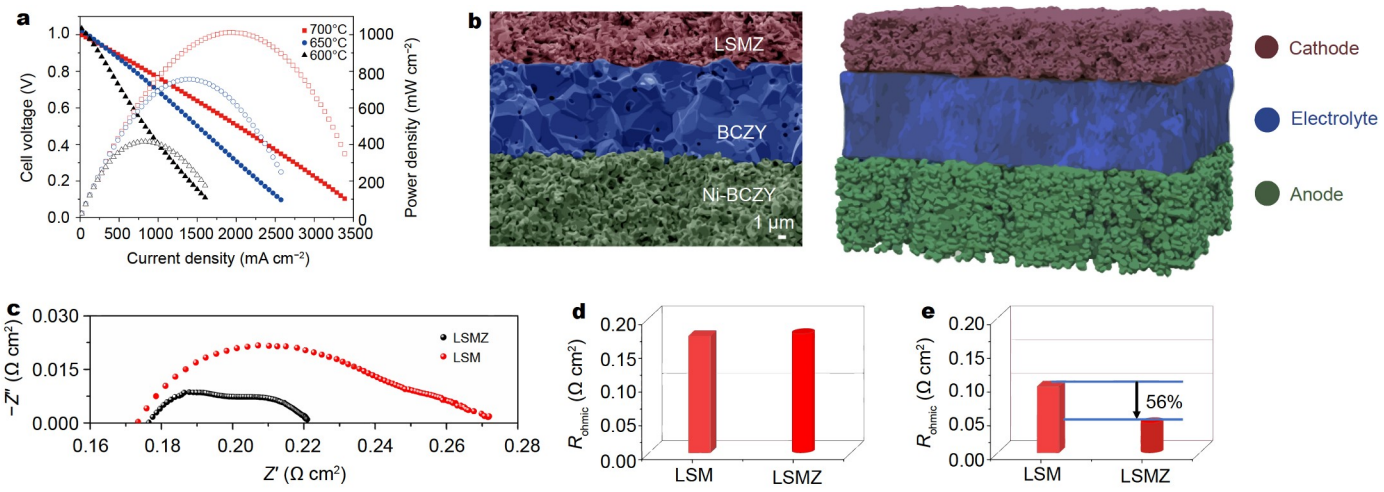

Figure 3 (a) *I-V* and power density curves for the cell using LSMZ cathode measured at different temperatures; (b) cross-sectional view for the LSMZ cell after testing (left) and the scheme for the tri-layer structure of the cell (right); (c) EIS plots of the LSM cell and the LSMZ cell measured at 700°C; comparison of the (d) Ohmic resistance (R_{ohmic}) and (e) polarization resistance (R_p) of the cells using LSM and LSMZ cathodes at 700°C.

Table 1 Comparison of the performance for H-SOFCs using LSM-based cathode reported in the literature and in this study. BZYZ: Zn-doped $BaZr_{0.85}Y_{0.15}O_{3-\delta}$; BZY: $BaZr_{0.8}Y_{0.2}O_{3-\delta}$; BCZY: $BaCe_{0.7}Zr_{0.1}Y_{0.2}O_{3-\delta}$.

Reference (year)	Cathode composition	Microstructure optimization (strategy)	Electrolyte and thickness	PPD (mW cm^{-2})
19 (2009)	$(La_{0.8}Sr_{0.2})_{0.98}MnO_3$	No	BZYZ, 5 μm	25 (800°C)
20 (2018)	$La_{0.8}Sr_{0.2}MnO_3$	Yes (ion impregnation)	BZY, 20 μm	200 (600°C)
30 (2020)	$La_{0.8}Sr_{0.2}MnO_3$	Yes (nanofiber)	BCZY, 15 μm	850 (700°C)
31 (2021)	$La_{0.5}Sr_{0.5}MnO_3$	No	BCZY, 15 μm	671 (700°C)
This study	$La_{0.5}Sr_{0.5}Mn_{0.875}Zn_{0.125}O_3$	No	BCZY, 15 μm	416 (600°C) 1012 (700°C)

0.099 Ω cm^2 at the testing temperature of 700°C, while the corresponding value for the LSMZ cell is 0.043 Ω cm^2 at the same testing temperature. The reduction is more than 50%, as illustrated in Fig. 3e. As stated above that both cells have a similar cell structure and use the same anode composition, the difference in R_p should primarily come from the different cathode materials utilized. Insights can be obtained by fitting the EIS plots with the equivalent circuit, as shown in Fig. S5. Three depressed semi-circles can be separated for the R_p of both LSM and LSMZ cells, meaning there are three major contributions at high frequency, middle frequency, and low frequency, respectively. The resistances at high frequency, middle frequency, and low frequency, named as R_{HF}, R_{MF} and R_{LF}, respectively, are listed in Table S2. One can find that the reduction of R_{HF} that is associated with the transfer of charge carriers [49,50] is profound when LSM is doped with Zn, decreasing from 0.06 to 0.013 Ω cm^2. It is known from the hydration tests and DFT calculations that the hydration and proton migration ability of LSMZ is better than that of LSM. Therefore, the improved proton migration and protonation can increase the transportation of the charge carrier (proton) at the reaction active area, thus leading to the decline of R_{HF} for LSMZ in comparison with that for the traditional LSM. The reduction of R_{MF} that is associated with the oxygen diffusion [49] is achieved by using LSMZ, and the result is consistent with the DFT calculation that Zn-doping lowers the formation energy of oxygen vacancy and helps the diffusion of oxygen-ions. In contrast to the dramatically decreased R_{HF} and R_{MF}, R_{LF} that is the reflection of transportation and adsorption of O_2 [39,51] for LSM and LSMZ is similar, being 0.028 and 0.026 Ω cm^2. It has been identified that both cells have similar microstructures, and the diffusion of O_2 is expected to be similar for both LSM and LSMZ cathode. Therefore, the similar R_{LF} value suggests the adsorption ability of O_2 for LSM and LSMZ is close. To demonstrate the hypothesis, the simulation of the O_2 adsorption on the surface of LSM and LSMZ was carried out by the DFT method. It is found that the adsorption energy for the O_2 adsorption at the LSM and LSMZ surfaces is −0.171 and −0.167 eV, respectively. The O_2 adsorption energy on LSM and LSMZ surface is very close, suggesting no apparent change in O_2 adsorption ability for LSM after Zn-doping, which could explain the reason for the similar R_{LF} of both LSM and LSMZ cathodes. The improved protonation, lower proton migration barrier, and better oxygen vacancy formation ability for Zn-doped LSM make the LSMZ cathode show a declined polarization resistance in R_{HF} and R_{MF} compared with the LSM cathode without Zn-doping and contribute to the much-decreased total R_p and thus larger power output for the LSMZ cell.

Besides the high fuel cell performance, stability is another critical issue that needs to be addressed. Although the good stability of LSM is well recognized, the stability of the LSM-based material with the incorporation of Zn is still unknown. In

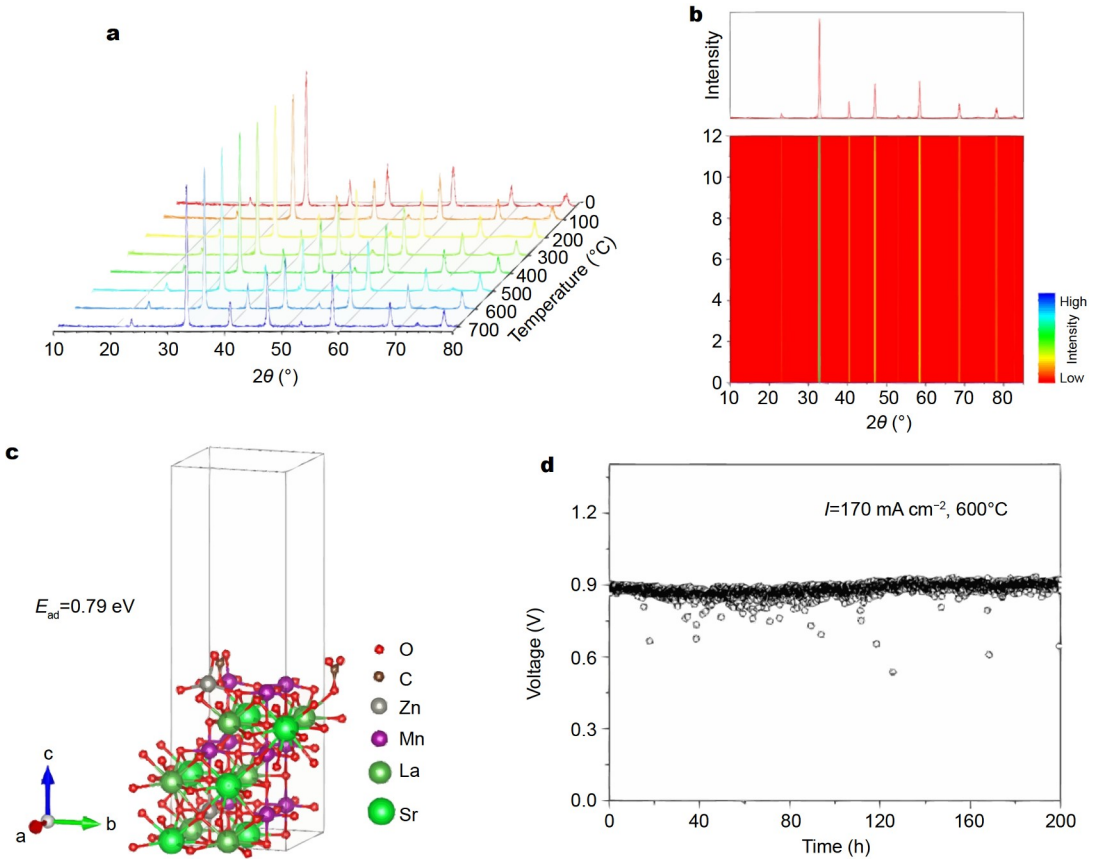

Figure 4 (a) *In-situ* XRD for the LSMZ tested at different temperatures under the CO_2-containing condition; (b) time course of XRD patterns measured at 600°C under the CO_2-containing condition; (c) the configuration of the LSMZ with adsorbed CO_2 and the adsorption energy (E_{ad}) is indicated; (d) long-term stability of the LSMZ cell under the fuel cell testing condition at 600°C.

order to answer this question, *in-situ* high-temperature XRD was performed to examine the stability of the LSMZ material under the CO_2-containing environment. The LSMZ material was tested at high temperatures under the condition of flowing 10% CO_2 (balanced with air), and XRD was employed to examine the phase composition of LSMZ at high temperatures under the CO_2-containing atmosphere. Two different methods were used to test the possible corrosion of CO_2 to LSMZ. One is to test the reactivity of CO_2 with LSMZ at different temperatures, and the other is to test the possible reaction of CO_2 with LSMZ as a function of time at a given temperature. No matter treating LSMZ from room temperature to 700°C (Fig. 4a) or keeping it at 600°C for 12 h (Fig. 4b), no detectable impurity can be found for the LSMZ. In addition, no change in the morphology for the LSMZ powders can be observed by scanning electron microscopy before and after the CO_2 treatment (Fig. S6), further suggesting its excellent chemical stability against CO_2. Therefore, it can be concluded that the doping of Zn into the lattice does not deteriorate the stability of the LSM-based material, and the LSMZ still has sufficient chemical stability. The DFT calculation was employed to reveal the mechanism for the high stability further. The adsorption of CO_2 on the LSMZ surface was simulated at the atomic level, and the result indicates that the adsorption energy of CO_2 on the surface of LSMZ is 0.79 eV. The energy is above zero, which means the adsorption of CO_2 on the LSMZ is unlikely to happen from the thermodynamical point of view [52]. The result agrees well with the experimental results, revealing LSMZ is thermodynamically stable with CO_2. Besides the tests of the chemical stability of the LSMZ itself, the operation stability of the LSMZ cell was also examined by running the LSMZ cell under the fuel cell testing condition for more than 200 h. No apparent degradation can be observed for the LSMZ cell during the whole test, suggesting the good stability of the cell. It has been known that the good stability of the LSM cathode makes it favorable for practical applications, whereas its reported poor performance makes it unfavorable for H-SOFCs. However, the doping of Zn into LSM can not only inherit good stability from traditional LSM but also improve the electrochemical performance greatly, serving as a promising cathode candidate for H-SOFCs.

CONCLUSIONS

In summary, LSM is the first-generation cathode suitable for traditional SOFCs working at high temperatures, but it is seldomly used for H-SOFCs due to its demonstrated low performance. To re-use LSM-based materials for H-SOFCs, the Zn-doping strategy is proposed, and the doping of Zn into LSM lattice can improve the cathode properties for the application in H-SOFCs, leading to high fuel cell performance. The mechanism behind this high fuel cell performance is clarified by using both theoretical approaches and experimental studies. The incorporation of Zn into the LSM cathode improves oxygen vacancy formation and protonation. As a result, the polarization resistance is reduced by more than 50%, leading to the improved fuel

cell performance from 622 mW cm^{-2} for the LSM cell to 1010 mW cm^{-2} for the LSMZ cell. Furthermore, the doping of Zn does not impair the stability of the material as well as the cell operation stability. As a result, the H-SOFC using the LSMZ cathode shows high fuel cell performance and good long-term stability, not only offering new and high-performing material for the LSM material family but also extending the application of traditional LSM-based material for H-SOFCs.

Received 6 July 2021; accepted 30 September 2021; published online 25 November 2021

1 Duan C, Kee RJ, Zhu H, *et al.* Highly durable, coking and sulfur tolerant, fuel-flexible protonic ceramic fuel cells. Nature, 2018, 557: 217–222
2 Medvedev DA, Lyagaeva JG, Gorbova EV, *et al.* Advanced materials for SOFC application: Strategies for the development of highly conductive and stable solid oxide proton electrolytes. Prog Mater Sci, 2016, 75: 38–79
3 Ding H, Wu W, Jiang C, *et al.* Self-sustainable protonic ceramic electrochemical cells using a triple conducting electrode for hydrogen and power production. Nat Commun, 2020, 11: 1907
4 Song Y, Chen Y, Wang W, *et al.* Self-assembled triple-conducting nanocomposite as a superior protonic ceramic fuel cell cathode. Joule, 2019, 3: 2842–2853
5 Chen Y, Yoo S, Pei K, *et al.* An *in situ* formed, dual-phase cathode with a highly active catalyst coating for protonic ceramic fuel cells. Adv Funct Mater, 2018, 28: 1704907
6 Li Y, Singh M, Zhuang Z, *et al.* Efficient reversible CO/CO_2 conversion in solid oxide cells with a phase-transformed fuel electrode. Sci China Mater, 2021, 64: 1114–1126
7 Jiang SP. Nanoscale and nano-structured electrodes of solid oxide fuel cells by infiltration: Advances and challenges. Int J Hydrogen Energy, 2012, 37: 449–470
8 Wachsman ED, Lee KT. Lowering the temperature of solid oxide fuel cells. Science, 2011, 334: 935–939
9 Zhang Y, Chen B, Guan D, *et al.* Thermal-expansion offset for high-performance fuel cell cathodes. Nature, 2021, 591: 246–251
10 Tarutin AP, Lyagaeva JG, Medvedev DA, *et al.* Recent advances in layered $Ln_2NiO_{4+\delta}$ nickelates: Fundamentals and prospects of their applications in protonic ceramic fuel and electrolysis cells. J Mater Chem A, 2021, 9: 154–195
11 Li J, Wang C, Wang X, *et al.* Sintering aids for proton-conducting oxides—a double-edged sword? A mini review. Electrochem Commun, 2020, 112: 106672
12 Cao D, Zhou M, Yan X, *et al.* High performance low-temperature tubular protonic ceramic fuel cells based on barium cerate-zirconate electrolyte. Electrochem Commun, 2021, 125: 106986
13 Duan C, Huang J, Sullivan N, *et al.* Proton-conducting oxides for energy conversion and storage. Appl Phys Rev, 2020, 7: 011314
14 Kilner JA, Burriel M. Materials for intermediate-temperature solid-oxide fuel cells. Annu Rev Mater Res, 2014, 44: 365–393
15 Saranya AM, Pla D, Morata A, *et al.* Engineering mixed ionic electronic conduction in $La_{0.8}Sr_{0.2}MnO_{3+\delta}$ nanostructures through fast grain boundary oxygen diffusivity. Adv Energy Mater, 2015, 5: 1500377
16 Graves C, Ebbesen SD, Jensen SH, *et al.* Eliminating degradation in solid oxide electrochemical cells by reversible operation. Nat Mater, 2015, 14: 239–244
17 Zhang X, Liu L, Zhao Z, *et al.* Enhanced oxygen reduction activity and solid oxide fuel cell performance with a nanoparticles-loaded cathode. Nano Lett, 2015, 15: 1703–1709
18 Painter AS, Huang YL, Wachsman ED. Durability of $(La_{0.8}Sr_{0.2})_{0.95}MnO_{3-\delta}$-$(Er_{0.2}Bi_{0.8})_2O_3$ composite cathodes for low temperature SOFCs. J Power Sources, 2017, 360: 391–398
19 Peng C, Melnik J, Li J, *et al.* ZnO-doped $BaZr_{0.85}Y_{0.15}O_{3-\delta}$ proton-conducting electrolytes: Characterization and fabrication of thin films. J Power Sources, 2009, 190: 447–452
20 Da'as EH, Bi L, Boulfrad S, *et al.* Nanostructuring the electronic conducting $La_{0.8}Sr_{0.2}MnO_{3-\delta}$ cathode for high-performance in proton-conducting solid oxide fuel cells below 600°C. Sci China Mater, 2018, 61: 57–64
21 Peng R, Wu T, Liu W, *et al.* Cathode processes and materials for solid oxide fuel cells with proton conductors as electrolytes. J Mater Chem, 2010, 20: 6218–6225
22 Muñoz-García AB, Pavone M. First-principles design of new electrodes for proton-conducting solid-oxide electrochemical cells: A-site doped $Sr_2Fe_{1.5}Mo_{0.5}O_{6-\delta}$ perovskite. Chem Mater, 2016, 28: 490–500
23 Xu X, Wang H, Fronzi M, *et al.* Tailoring cations in a perovskite cathode for proton-conducting solid oxide fuel cells with high performance. J Mater Chem A, 2019, 7: 20624–20632
24 Zohourian R, Merkle R, Raimondi G, *et al.* Mixed-conducting perovskites as cathode materials for protonic ceramic fuel cells: Understanding the trends in proton uptake. Adv Funct Mater, 2018, 28: 1801241
25 Xu X, Xu Y, Ma J, *et al.* Tailoring electronic structure of perovskite cathode for proton-conducting solid oxide fuel cells with high performance. J Power Sources, 2021, 489: 229486
26 Xu X, Bi L, Zhao XS. Highly-conductive proton-conducting electrolyte membranes with a low sintering temperature for solid oxide fuel cells. J Membrane Sci, 2018, 558: 17–25
27 Bi L, Shafi SP, Da'as EH, *et al.* Tailoring the cathode-electrolyte interface with nanoparticles for boosting the solid oxide fuel cell performance of chemically stable proton-conducting electrolytes. Small, 2018, 14: 1801231
28 Wang B, Liu X, Bi L, *et al.* Fabrication of high-performance proton-conducting electrolytes from microwave prepared ultrafine powders for solid oxide fuel cells. J Power Sources, 2019, 412: 664–669
29 Kresse G, Furthmüller J. Efficient iterative schemes for *ab initio* total-energy calculations using a plane-wave basis set. Phys Rev B, 1996, 54: 11169–11186
30 Blöchl PE, Jepsen O, Andersen OK. Improved tetrahedron method for brillouin-zone integrations. Phys Rev B, 1994, 49: 16223–16233
31 Xu Y, Xu X, Cao N, *et al.* Perovskite ceramic oxide as an efficient electrocatalyst for nitrogen fixation. Int J Hydrogen Energy, 2021, 46: 10293–10302
32 Tao Z, Xu X, Bi L. Density functional theory calculations for cathode materials of proton-conducting solid oxide fuel cells: A mini-review. Electrochem Commun, 2021, 129: 107072
33 Ji Q, Xu X, Liu X, *et al.* Improvement of the catalytic properties of porous lanthanum manganite for the oxygen reduction reaction by partial substitution of strontium for lanthanum. Electrochem Commun, 2021, 124: 106964
34 Muñoz-García AB, Tuccillo M, Pavone M. Computational design of cobalt-free mixed proton-electron conductors for solid oxide electrochemical cells. J Mater Chem A, 2017, 5: 11825–11833
35 Zhang X, Pei C, Chang X, *et al.* FeO_6 octahedral distortion activates lattice oxygen in perovskite ferrite for methane partial oxidation coupled with CO_2 splitting. J Am Chem Soc, 2020, 142: 11540–11549
36 Ren R, Wang Z, Meng X, *et al.* Tailoring the oxygen vacancy to achieve fast intrinsic proton transport in a perovskite cathode for protonic ceramic fuel cells. ACS Appl Energy Mater, 2020, 3: 4914–4922
37 Kreuer KD. Proton-conducting oxides. Annu Rev Mater Res, 2003, 33: 333–359
38 Parbey J, Wang Q, Lei J, *et al.* High-performance solid oxide fuel cells with fiber-based cathodes for low-temperature operation. Int J Hydrogen Energy, 2020, 45: 6949–6957
39 Dai H, Xu X, Liu C, *et al.* Tailoring a $LaMnO_3$ cathode for proton-conducting solid oxide fuel cells: Integration of high performance and excellent stability. J Mater Chem A, 2021, 9: 12553–12559
40 Wang Q, Hou J, Fan Y, *et al.* $Pr_2BaNiMnO_{7-\delta}$ double-layered Ruddlesden-Popper perovskite oxides as efficient cathode electrocatalysts for low temperature proton conducting solid oxide fuel cells. J Mater Chem A, 2020, 8: 7704–7712
41 Li J, Hou J, Lu Y, *et al.* Ca-containing $Ba_{0.95}Ca_{0.05}Co_{0.4}Fe_{0.4}Zr_{0.1}Y_{0.1}O_{3-\delta}$ cathode with high CO_2-poisoning tolerance for proton-conducting solid oxide fuel cells. J Power Sources, 2020, 453: 227909
42 Bu Y, Joo S, Zhang Y, *et al.* A highly efficient composite cathode for

proton-conducting solid oxide fuel cells. J Power Sources, 2020, 451: 227812
43 Zhang Y, Zhu A, Guo Y, *et al.* Electrochemical performance and effect of moisture on $Ba_{0.5}Sr_{0.5}Sc_{0.175}Nb_{0.025}Co_{0.8}O_{3-\delta}$ oxide as a promising electrode for proton-conducting solid oxide fuel cells. Appl Energy, 2019, 238: 344–350
44 Xia Y, Jin Z, Wang H, *et al.* A novel cobalt-free cathode with triple-conduction for proton-conducting solid oxide fuel cells with unprecedented performance. J Mater Chem A, 2019, 7: 16136–16148
45 Pikalova E, Kolchugin A, Koroleva M, *et al.* Functionality of an oxygen $Ca_3Co_4O_{9+\delta}$ electrode for reversible solid oxide electrochemical cells based on proton-conducting electrolytes. J Power Sources, 2019, 438: 226996
46 Xie Y, Shi N, Huan D, *et al.* A stable and efficient cathode for fluorine-containing proton-conducting solid oxide fuel cells. ChemSusChem, 2018, 11: 3423–3430
47 Huan D, Shi N, Zhang L, *et al.* New, efficient, and reliable air electrode material for proton-conducting reversible solid oxide cells. ACS Appl Mater Interfaces, 2018, 10: 1761–1770
48 Choi S, Kucharczyk CJ, Liang Y, *et al.* Exceptional power density and stability at intermediate temperatures in protonic ceramic fuel cells. Nat Energy, 2018, 3: 202–210
49 Fabbri E, Bi L, Pergolesi D, *et al.* High-performance composite cathodes with tailored mixed conductivity for intermediate temperature solid oxide fuel cells using proton conducting electrolytes. Energy Environ Sci, 2011, 4: 4984–4993
50 He F, Wu T, Peng R, *et al.* Cathode reaction models and performance analysis of $Sm_{0.5}Sr_{0.5}CoO_{3-\delta}$-$BaCe_{0.8}Sm_{0.2}O_{3-\delta}$ composite cathode for solid oxide fuel cells with proton conducting electrolyte. J Power Sources, 2009, 194: 263–268
51 Kournoutis VC, Tietz F, Bebelis S. AC impedance characterisation of a $La_{0.8}Sr_{0.2}Co_{0.2}Fe_{0.8}O_3$ electrode. Fuel Cells, 2009, 9: 852–860
52 Lu X, Yang X, Jia L, *et al.* First principles study on the oxygen reduction reaction of the $La_{1-x}Sr_xMnO_3$ coated $Ba_{1-x}Sr_xCo_{1-y}Fe_yO_3$ cathode for solid oxide fuel cells. Int J Hydrogen Energy, 2019, 44: 16359–16367

Acknowledgements This work was supported by the National Natural Science Foundation of China (51972183 and 51972128) and the Startup Funding for Talents at the University of South China.

Author contributions Wu S and Bi L designed this study. Wu S and Li X performed the experiments. Xu X performed the DFT calculations and analyzed the data. Bi L wrote the manuscript with other co-authors and all authors discussed the results and provided their approval to the final version.

Conflict of interest The authors declare that they have no conflict of interest.

Supplementary information Supporting data are available in the online version of the paper.

Shuai Wu is a postgraduate student, studying in the group of Professor Lei Bi. His research interest is the utilization of the doping strategy to tailor cathode materials for H-SOFCs with enhanced performance. Designing new cathode materials with protonation ability is now his major research topic.

Xi Xu was a master student in the group of Professor Lei Bi and now she is a PhD student at Imperial College London and doing her research in the laboratory of Professor Stephen Skinner from October 2020. Her current research topic is the development of advanced cathode materials for H-SOFCs, which covers both the experimental part and the theoretical simulation part using density functional theory (DFT).

Xiaomei Li is a postgraduate student in the group of Professor Lei Bi. After joining the group, she started the work of developing high-performing H-SOFCs, by microstructure optimizations and design of new materials. She is also interested in understanding the electrode working mechanisms for H-SOFCs.

Lei Bi is now a full professor at the University of South China, leading a group working on H-SOFCs. After obtaining his PhD degree from the University of Science and Technology of China, he spent six years working at the National Institute for Materials Science in Japan as a postdoc and King Abdullah University of Science and Technology in Saudi Arabia as a research scientist. His research interests are the development of H-SOFCs, using both the first-principles calculation method and experimental approaches.

通过Zn调节第一代Sr掺杂的$LaMnO_3$阴极制备高性能质子导体固体氧化物燃料电池

吴帅[1,3†], 许茜[2†], 李晓梅[1,3], 毕磊[1*]

摘要 Sr掺杂的$LaMnO_3$ (LSM)是固体氧化物燃料电池(SOFC)的第一代阴极. 为了提高其质子化能力从而应用于质子导体SOFC(H-SOFC), 本研究成功合成了Zn和Sr共掺杂的$LaMnO_3$材料(LSMZ), 即通过Zn离子调节LSM的性能. 第一性原理研究表明, LSMZ提高了材料的质子化能力, 而且降低了材料中氧空位的形成能, 使LSMZ在电池应用中展现出较高的性能, 是文献报道同类阴极在H-SOFC中的最大值. 此外, 良好的燃料电池性能并没有影响材料的稳定性. 原位CO_2腐蚀测试和第一性原理计算表明LSMZ材料对于CO_2具有高稳定性, 使LSMZ电池在工作状态下具有较好的长期稳定性. Zn掺杂策略将传统LSM阴极的高稳定性与高性能相结合, 将LSM阴极带回到中温工作区间.

